4

Thermo - Physical Properties of Iron - Magnesium Alloys

Krisztina Kádas[1,2], Hualei Zhang[1], Börje Johansson[1,3], Levente Vitos[1,2,3] and Rajeev Ahuja[1,2]
[1]*KTH Royal Institute of Technology*
[2]*Research Institute for Solid State Physics and Optics*
[3]*Uppsala University*
[1,3]*Sweden*
[2]*Hungary*

1. Introduction

According to the common phase diagrams, iron and magnesium are almost immiscible at ambient pressure Massalski (1986). In the liquid phase, the solubility of Mg in Fe is of the order of 0.025 atomic percent (at.%). The maximum solid solubility of Fe in Mg is 0.00041 at.% and the Fe content in Mg at the eutectic point is less than 0.008 at.% (Haitani et al., 2003). Below 1273 K the solubility of Mg in α-Fe is below the detection limit and about 0.25 at.% Mg can be solved in $\delta-$Fe at the monotectic temperature. The immiscibility of Fe and Mg at ambient conditions is in line with the well-known Hume-Rothery rules, according to which more than 15% atomic size difference between alloy constituents hinders solid solution formation (Massalski, 1996). In spite of the negligible solubility of Mg in Fe, several Fe-rich metastable Fe-Mg solid solution have been synthesized.

According to the pioneering work by Hightower *et al.* (Hightower et al., 1997), mechanical alloying produced Fe-Mg substitutional solid solutions with up to 20 at.% Mg and having the body centered cubic (bcc) crystallographic phase of α-Fe. Later, using the similar alloying procedure, Dorofeev *et al.* (Dorofeev et al., 2004; Yelsukov et al., 2005) found that about $5-7$ at.% Mg in α-Fe forms supersaturated solid solution. These authors suggested that the driving force for the formation of Fe-Mg solid solutions is associated with the excess energy of coherent interfaces in the Fe-Mg nanocomposite, which facilitates incorporation of Mg into α-Fe. Indeed, based on semiempirical thermodynamic calculations, Yelsukov *et al.* (Yelsukov et al., 2005) obtained 6 kJ/mol for the enthalpy of formation for Fe-Mg solid solutions, compared to 20 kJ/mol calculated for the corresponding Fe-Mg nanocomposites. In addition to the mechanical alloying techniques, pressure was also found to facilitate the solid solution formation between Fe and Mg. Dubrovinskaia *et al.* (Dubrovinskaia et al., 2004) reported that at pressures around 20 GPa and temperatures up to 2273 K, the solubility of Mg in bcc Fe was increased to 4 at.%. They found that the lattice parameter of the bcc Fe-Mg alloy increased approximately by 0.6 % per at.% Mg. Furthermore, recent experimental measurements in combination with theoretical simulations demonstrated that at the megabar pressure range more than 10 at.% Mg could be dissolved in liquid Fe, which then could be quenched to ambient conditions (Dubrovinskaia et al., 2005). The mechanism behind the

high-pressure alloying is the much larger compressibility of Mg compared to that of Fe.
Most of the theoretical and experimental investigations of the Fe-Mg solid solutions so far focused on the phase diagram, crystallographic structure, nanostructure, grain boundaries and segregation. However, much less is known about the mechanical properties of Fe-rich Fe-Mg alloys. Here we present a systematic first-principles study of the effect of Mg on the elastic properties of ferromagnetic bcc Fe-Mg alloys. We calculate the single-crystal and polycrystalline elastic parameters by using the all-electron exact muffin-tin orbitals method (Andersen et al., 1994; Vitos et al., 2000; Vitos, 2001) in combination with the coherent-potential approximation (Soven, 1967; Gyorffy, 1972; Vitos et al., 2001; Vitos, 2007). Since at ambient conditions, the Fe-rich Fe-Mg alloys were found to adopt the ferromagnetic bcc structure (Hightower et al., 1997; Dorofeev et al., 2004; Dubrovinskaia et al., 2005), all calculations are performed for this magnetic and crystallographic phase. Using Mösbauer spectroscopy, Hightower *et al.* (Hightower et al., 1997) found that bcc Fe-Mg alloys encompassing ~ 18 at.% Mg possess large chemical heterogeneities. According to that study only few Fe atoms have Mg atoms as first-nearest neighbors and the Mg atoms cluster into Fe-depleted zones on the bcc lattice. On the other hand, Dorofeev *et al.* (Dorofeev et al., 2004; Yelsukov et al., 2005) determined the effect of nearest neighbor and next nearest neighbor Mg atom on the hyperfine magnetic field of Fe nuclei in Fe-Mg alloys containing $5-7$ at.% Mg. Moreover, the $Fe_{0.96}Mg_{0.04}$ synthesized by Dubrovinskaia *et al.* (Dubrovinskaia et al., 2004) at high temperature and moderate pressures was reported to be homogeneous. It is also noticeable the excellent agreement obtained between the experimental and theoretical equation of states for $Fe_{0.96}Mg_{0.04}$, the latter obtained for completely random alloy (Dubrovinskaia et al., 2005). These findings indicate that clustering of Mg atoms is less significant in Fe-rich alloys. Because of that, we limit the present study to $Fe_{1-x}Mg_x$ alloys with $0 \leq x \leq 0.1$ and assume random distributions of the Mg atoms on the parent lattice.
In order to be able to assess the results obtained for Fe-Mg alloys at ambient condition, here we also present some results obtained for random $Fe_{1-x}Cr_x$ alloys with $0 \leq x \leq 0.1$. It is well-known that Fe-Cr constitute the basis for stainless steels. The Fe-Cr alloys, except the high temperature Fe-rich γ-phase and the σ-phase observed around equimolar concentrations, adopt the bcc structure (Hultgren et al., 1973). At normal operating temperatures, these bcc alloys are ferromagnetic with Curie temperatures around $900-1050$ K (Hultgren et al., 1973). For $x \lesssim 0.1$ and $T \gtrsim 600$ K, the Fe-Cr system is fully miscible, whereas the nucleation or spinodal (α') decomposition driven clustering occurs at higher Cr concentrations (Tavaresa et al., 2001; Cieslak et al., 2000). Nevertheless, it has been shown (Olsson et al., 2003; 2006) that the energetics of Fe-Cr alloys with $\lesssim 20$ at.% Cr are well described using the substitutional disordered ferromagnetic bcc phase.
The composition and the structure of the Earth's solid inner core are still unknown. The core is considered to be made of iron-rich alloys containing 5-15% nickel (Anderson, 1989) and one or more light elements (McDonough, 2003). Based on seismic observations, different models have been constructed to describe the physical properties of the Earth's interior. The most widely accepted of these models is the "Preliminary Reference Earth Model" (PREM, (Dziewonski & Anderson, 1981)), which provides the radial distribution of elastic properties, seismic quality factors and densities. The physical properties of pure iron at core conditions have been extensively studied both experimentally (Singh et al., 1998; Mao et al., 1998; Dubrovinsky et al., 2000) and theoretically (Stixrude & Cohen, 1995; Söderlind et al., 1996; Steinle-Neumann et al., 1999; Laio et al., 2000; Vočadlo et al., 2000; Steinle-Neumann et al., 2001; Belonoshko et al., 2003; Qiu & Marcus, 2003; Belonoshko et al., 2007), and they have

been found to differ significantly from those of the PREM model. In 2001, Hemley and Mao proposed that pure iron has a nonmagnetic hexagonal closed-packed (hcp) structure (ϵ-Fe) at Earth's core pressures and temperatures (Hemley & Mao, 2001). Lately, the body-centered cubic (bcc) phase of iron was suggested to be present in the inner core, (Ross et al., 1990; Matsui & Anderson, 1997; Belonoshko et al., 2003; 2007; 2008), although its stability at core conditions is still in discussion (Vočadlo et al., 2003; Vočadlo, 2007). It has been shown recently (Mikhaylushkin et al., 2007) that because of the subtle energy difference between the different phases of Fe at core conditions, the presence of any of the hcp, face-centered cubic (fcc) or bcc phases can not be ruled out in the Earth's inner core.

The higher density of pure iron compared to that of the Earth's core indicates the presence of light element(s) in this region. In the past few years, notable effort has been made to study iron-rich alloys at core conditions, covering nickel (Vočadlo et al., 2006; Kantor et al., 2007; Dubrovinsky et al., 2007), silicon (Lin et al., 2002; Vočadlo et al., 2003; Chen et al., 2007) and sulphur (Vočadlo et al., 2003; Chen et al., 2007) as alloying elements. However, none of these proposed composition models were in full agreement with seismic observations.

Magnesium, one of the most abundant of Earth elements, which does not alloy with iron at ambient conditions, has just recently been proposed as a possible component of the Earth's core, when Dubrovinskaia et al. have shown that high pressure promotes the solubility of Mg in iron (Dubrovinskaia et al., 2004; 2005). On the other hand, today, magnesium is often classified as a litophile element (McDonough & Sun, 1995; Allegre et al., 1995), and therefore its presence in the core is precluded. This classification is based on two main arguments. First, it is believed that the consistency between the relative amount of Mg in the Earth's mantle and in the chondritic models, makes the occurrence of Mg in the core unlikely. Second, it is thought that metallic Mg in the core would require extremely reducing conditions. Indeed, based on oxygen fugacity, the occurrence of metallic Mg is rather improbable (Robie et al., 1978) at mantle conditions. However, the oxygen fugacity significantly increases with increasing temperature for Mg, indicating that at inner core conditions the presence of Mg should not be ruled out (Robie et al., 1978). Furthermore, the ionic character of metal oxides at the extreme conditions of the core, is not yet fully understood. In addition, Si, which also has lower oxygen fugacity, than the redox state of the Earth's mantle, is widely accepted as a possible component of the inner core.

Recently we showed that Mg is a strong candidate light element of the inner core (Kádas et al., 2008a; Kádas, Vitos, Johansson & Ahuja, 2009). Here, without examining the partition of Mg into the core, we describe the thermo-physical properties of hcp and bcc iron-magnesium alloys at the conditions of the Earth's inner core. We demonstrate the effect of Mg alloying on the hexagonal axial ratio, elastic constants, density and sound wave velocities, and show that the shear modulus and the transverse sound velocity of hcp Fe are notably reduced by Mg (Kádas et al., 2008a). Though the calculated shear moduli and sound velocities of hcp Fe-Mg alloys still differ significantly from those of the core as provided by seismic observations, even at 10 atomic % Mg content, Mg alloying changes the elastic properties of hcp iron in such a way that the differences to the seismic data decrease. At core conditions, we predict that 5-10% Mg stabilizes bcc Fe both dynamically and thermodynamically (Kádas, Vitos, Johansson & Ahuja, 2009), and we give an electronic structure explanation of this phenomenon. We demonstrate that the physical properties of bcc Fe-Mg alloys containing 5-10% Mg in fact reproduce those of the inner core: the calculated density, elastic moduli and sound velocities of bcc Fe-Mg alloys are consistent with seismic data. Therefore the bcc-structured Fe-Mg alloy seems to be amongst the strongest candidate models for the Earth's solid inner core.

2. Theory

2.1 Computational method

The present calculations are based on density functional theory (DFT) (Hohenberg & Kohn, 1964) formulated within the Perdew-Burke-Ernzerhof generalized gradient approximation for the exchange-correlation functional (Perdew et al., 1996). The Kohn-Sham equations (Kohn & Sham, 1965) were solved using the exact muffin-tin orbitals (EMTO) method (Andersen et al., 1994; Vitos et al., 2000; Vitos, 2001). The substitutional disorder was treated within the coherent-potential approximation (CPA) (Soven, 1967; Gyorffy, 1972; Vitos et al., 2001; Vitos, 2007). From the self-consistent charge density the total energy was calculated using the full-charge density technique (Kollár et al., 2000).

The EMTO method is an improved screened Korringa-Kohn-Rostoker method (Andersen et al., 1994), where the full potential is represented by overlapping muffin-tin potential spheres. By using overlapping spheres one describes more accurately the exact crystal potential, when compared to the conventional muffin-tin or non overlapping methods (Andersen et al., 1998; Vitos, 2001). Further details about the EMTO method and its self-consistent implementation can be found in Refs. (Vitos et al., 2000; Andersen et al., 1994; Vitos, 2001; Vitos et al., 2001; Vitos, 2007). The EMTO approach ensures the accuracy needed for the calculations of anisotropic lattice distortions in random alloys. It has been applied successfully in the *ab initio* study of the thermo-physical properties of random Fe-based alloys (Vitos et al., 2002; 2003; Olsson et al., 2003; Vitos et al., 2006; Dubrovinskaia et al., 2005; Kádas et al., 2008a; Kádas, Vitos, Johansson & Ahuja, 2009; Zhang et al., 2009; 2010), simple and transition metal alloys (Taga et al., 2005; Huang et al., 2006; Zander et al., 2007; Vitos, 2001; Magyari-Köpe, Grimvall & Vitos, 2002; Magyari-Köpe et al., 2004; Ahuja et al., 2009; Delczeg-Czirjak et al., 2009; Kádas, Lindquist, Erikssson, Johansson & Vitos, 2009; Sahlberg et al., 2009) and solid solutions (Magyari-Köpe et al., 2001; Magyari-Köpe, Vitos, Johansson & Kollár, 2002; Landa et al., 2002; Magyari-Köpe, Vitos, G. Grimvall & Kollár, 2002; Hu et al., 2007; Kádas et al., 2008b; Hu et al., 2008).

2.2 Calculation of elastic constants

2.2.1 Body-centered cubic elastic constants

There are three independent elastic constants in a body centered cubic system: C_{11}, C_{12} and C_{44}. They can be obtained by calculating the total energy as a function of small strains δ applied on the parent lattice. In the present application, the cubic shear constant, $C' = (C_{11} - C_{12})/2$ was obtained using volume-conserving orthorhombic deformation,

$$\begin{bmatrix} \delta_{\mathrm{o}} & 0 & 0 \\ 0 & -\delta_{\mathrm{o}} & 0 \\ 0 & 0 & \frac{\delta_{\mathrm{o}}^2}{1-\delta_{\mathrm{o}}^2} \end{bmatrix}. \tag{1}$$

and C' was determined from $\Delta E_{\mathrm{o}} = 2VC'\delta_{\mathrm{o}}^2 + \mathrm{O}(\delta_{\mathrm{o}}^4)$.

Applying the monoclinic strain

$$\begin{bmatrix} 0 & \delta_{\mathrm{m}} & 0 \\ \delta_{\mathrm{m}} & 0 & 0 \\ 0 & 0 & \frac{\delta_{\mathrm{m}}^2}{1-\delta_{\mathrm{m}}^2} \end{bmatrix}, \tag{2}$$

C_{44} was calculated from $\Delta E_{\mathrm{m}} = 2VC_{44}\delta_{\mathrm{m}}^2 + \mathrm{O}(\delta_{\mathrm{m}}^4)$.

C_{11} and C_{12} were separated by using C' and the cubic bulk modulus $B = (C_{11} + 2C_{12})/3$.

2.2.2 Hexagonal closed-packed elastic constants

In a hexagonal closed-packed system there are five independent elastic constants: $C_{11}, C_{12}, C_{13}, C_{33}$ and C_{44}. They were obtained from the bulk modulus,

$$B = \frac{C_{33}(C_{11} + C_{12}) - 2C_{13}^2}{C_S}, \tag{3}$$

where $C_S = C_{11} + C_{12} + 2C_{33} - 4C_{13}$, the logarithmic volume derivative of the hexagonal lattice parameter,

$$\frac{d\ln(c/a)_0}{d\ln V} = -\frac{C_{33} - C_{11} - C_{12} + C_{13}}{C_S}, \tag{4}$$

and three isochoric strains (Steinle-Neumann et al., 1999). By varying the c/a ratio at a given volume and applying the strain

$$\begin{bmatrix} \delta_{\mathrm{h}} & 0 & 0 \\ 0 & \delta_{\mathrm{h}} & 0 \\ 0 & 0 & \frac{1}{(1+\delta_{\mathrm{h}})^2} - 1 \end{bmatrix}, \tag{5}$$

C_S was calculated from $\Delta E_{\mathrm{h}} = VC_S\delta^2 + \mathrm{O}(\delta^3)$, where δ is the magnitude of the strain, and $\Delta E_{\mathrm{h}} = E(\delta_{\mathrm{h}}) - E(0)$ is the energy difference of the strained and unstrained systems. To determine $C_{66} = (C_{11} - C_{12})/2$, we applied an orthorhombic strain

$$\begin{bmatrix} \delta_{\mathrm{o}} & 0 & 0 \\ 0 & -\delta_{\mathrm{o}} & 0 \\ 0 & 0 & \frac{\delta_{\mathrm{o}}^2}{1-\delta_{\mathrm{o}}^2} \end{bmatrix}, \tag{6}$$

leading to the energy change $\Delta E_{\mathrm{o}} = 2VC_{66}\delta_{\mathrm{o}}^2 + \mathrm{O}(\delta_{\mathrm{o}}^4)$. Applying the monoclinic strain

$$\begin{bmatrix} 0 & 0 & \delta_{\mathrm{m}} \\ 0 & \frac{\delta_{\mathrm{m}}^2}{1-\delta_{\mathrm{m}}^2} & 0 \\ \delta_{\mathrm{m}} & 0 & 0 \end{bmatrix}, \tag{7}$$

C_{44} was determined from $\Delta E_{\mathrm{m}} = 2VC_{44}\delta_{\mathrm{m}}^2 + \mathrm{O}(\delta_{\mathrm{m}}^4)$.

2.2.3 Polycrystalline elastic constants

There are several different techniques for averaging the single-crystal data. We use Hill (Hill, 1952) averaging method to investigate the polycrystalline bulk (B) and shear moduli (G). According to the Hill averaging method, the polycrystalline B and G are given as the arithmetic average of the Voigt (Voigt, 1889) and Reuss (Reuss, 1929) limits. In the crystal aggregates, Voigt method assumed a uniform strain, while Reuss proposed a uniform stress. Accordingly, for a cubic crystal, the polycrystalline shear modulus is

$$\begin{aligned} G &= (G_{\mathrm{V}} + G_{\mathrm{R}})/2, \\ G_{\mathrm{R}} &= 5(C_{11} - C_{12})C_{44}(4C_{44} + 3C_{11} - 3C_{12})^{-1}, \\ G_{\mathrm{V}} &= (C_{11} - C_{12} + 3C_{44})/5. \end{aligned} \tag{8}$$

where the G_{R} and G_{V} are the Reuss and Voigt bounds, respectively.

For cubic crystal, the Voigt and Reuss bounds are identical with the single-crystal bulk modulus, i.e.,

$$\begin{aligned} B &= (B_{\mathrm{V}} + B_{\mathrm{R}})/2, \\ B_{\mathrm{R}} = B_{\mathrm{V}} &= (C_{11} + 2C_{12})/3, \end{aligned} \tag{9}$$

Using a variational method, Hashin and Shtrikman (Hashin & Shtrikman, 1962) derived more rigorous upper and lower bounds for B and G. For cubic lattices with $C' < C_{44}$, these bounds are

$$\begin{aligned} B_{\mathrm{u}} = B_{\mathrm{u}} &= \frac{C_{11} + 2C_{12}}{3}, \\ G_{\mathrm{l}} &= C' + 3\left(\frac{5}{C_{44} - C'} + 4\beta_1\right)^{-1}, \\ G_{\mathrm{u}} &= C_{44} + 2\left(\frac{5}{C' - C_{44}} + 6\beta_2\right)^{-1}, \end{aligned} \tag{10}$$

where

$$\begin{aligned} \beta_1 &= \frac{3(B + 2C')}{5C'(3B + 4C')}, \\ \beta_2 &= \frac{3(B + 2C_{44})}{5C_{44}(3B + 4C_{44})}. \end{aligned} \tag{11}$$

For $C' > C_{44}$, the upper and lower bounds are reversed.

2.3 Application to iron-magnesium systems

The cubic elastic constants of the random ferromagnetic bcc $Fe_{1-x}Mg_x$ ($0 \leq x \leq 0.1$) alloys at ambient conditions were calculated as a function of the chemical composition. At each concentration the theoretical equilibrium volume and the bulk modulus were derived from an exponential Morse type function (Moruzzi et al., 1988) fitted to the *ab initio* total energies of bcc structures calculated for seven different atomic volumes. In order to obtain the two cubic shear moduli C' and C_{44}, we used volume-conserving orthorhombic and monoclinic deformations as described, e.g., in Ref. (Vitos, 2007).

The polycrystalline Young's modulus (E) and the Poisson ratio (ν) are connected to B and G by the relations

$$\begin{aligned} E &= 9BG/(3B + G), \\ \nu &= (3B - 2G)/(6B + 2G). \end{aligned} \tag{12}$$

Finally, the polycrystalline elastic Debye temperature (Θ) was calculated from the longitudinal and transversal sound velocities obtained from B, G, and the average alloy density (see, e.g., Ref.(Vitos, 2007)).

In the present electronic structure and total energy calculations, the one-electron equations were solved within the scalar-relativistic and soft-core approximations. The Green function was calculated for 16 complex energy points distributed exponentially on a semicircular contour. In the basis set we included s, p, d, and f orbitals ($l_{max} = 3$), and the one-center expansion of the full charge density was truncated at $l^h_{max} = 8$ (Vitos, 2007). The electrostatic correction to the single-site coherent potential approximation was described using the

screened impurity model (Korzhavyi et al., 1995) with screening parameter of 0.6. The radii of the overlapping muffin-tin spheres of Fe, Mg, and Cr were chosen to be equal to the average atomic sphere radius.
To calculate the two cubic shear constants, C' and C_{44}, for bcc iron-magnesium alloys at core conditions, the total energy was computed for six different orthorhombic and monoclinic distortions ($\delta_{o/m}$=0.00, 0.01, ..., 0.05). The bulk modulus was determined from an exponential Morse-type function (Moruzzi et al., 1988) fitted to the total energies of the non-distorted bcc structure (δ=0) calculated for 10 different volumes. Finally, C_{11} and C_{12} were separated by using C' and the cubic bulk modulus B.
To determine the elastic constants for hcp iron-magnesium alloys, the total energy was calculated for six different orthorhombic and monoclinic distortions ($\delta_{o/m}$=0.00, 0.01, ..., 0.05) to determine C_{66} and C_{44}, respectively, and for nine hexagonal distortions ($\delta_h = -0.04, -0.03, ..., 0.00, ..., 0.04$) to obtain C_S. The sound velocities were determined by solving the secular equation, as it is given by Grimvall (Grimvall, 1999).
The temperature effect in the elastic constants calculated at fixed volume was taken into account via the Fermi-Dirac distribution of the electrons and neglecting the phonon contributions. We used the Debye model to account for the lattice vibration effects in the Gibbs energy. In the self-consistent EMTO calculations, the one-electron equations were treated within the scalar relativistic and soft core approximations. The EMTO Green's function was calculated for 16 energy points. In the EMTO basis set s, p, d and f orbitals were included for both hcp and bcc Fe-Mg systems. In the case of the strained hcp structures 9744 $k-$points were used in the irreducible part of monoclinic Brillouin zones. For the strained bcc structures, 22000 k-points were used in the irreducible part of the monoclinic Brillouin zones. The Hashin-Shtrikman averages (Hashin & Shtrikman, 1962) were applied to calculate the shear and Young moduli, and the sound velocities of bcc Fe-Mg alloys at Earth's core conditions. The total charge density was expanded in spherical harmonics, including terms up to l_{max}=10.

3. Iron-magnesium alloys at ambient conditions

In this chapter we review the thermo-physical properties of ferromagnetic body-centered cubic iron-magnesium alloys at ambient conditions.

3.1 Equation of state and formation energy

In this section, we investigate the composition dependence of the equation of state and formation energy of ferromagnetic bcc $Fe_{1-x}Mg_x$ ($0 \leq x \leq 0.1$) random alloys. For comparison, we also show results obtained for Fe-Cr alloys. The composition dependence of $a(x)$ is shown in Fig. 1 (left panel) along with the experimental data for Fe-Mg (Hightower et al., 1997; Dorofeev et al., 2004) and Fe-Cr (Sutton & Hume-Rothery, 1955; Pearson, 1958). Compared to slight increase on bcc Fe by Cr, Mg strongly enlarge lattice parameter of bcc Fe as shown in Fig. 1 (left panel).
Since the lattice constant of bcc Fe is by ~ 0.019 Å smaller than that of B2 Cr, based on Vegard's rule we would predict a linear $a(x)$ with slope of $\Delta a(x)/\Delta x \sim 0.2 \times 10^{-3}$ Å per at.% Cr. However, both the experimental and the theoretical lattice parameters deviate from this simple linear trend as shown in Fig. 1 (left panel). The EMTO lattice parameter reaches a maximum value between 7.5 and 10 at.% Cr and remains above the lattice parameter of pure Fe for all concentrations considered here. Using the theoretical values below $c = 0.1$, the theoretical slope of $a(x) \sim 1.7 \times 10^{-3}$ Å is larger than the average experimental value of

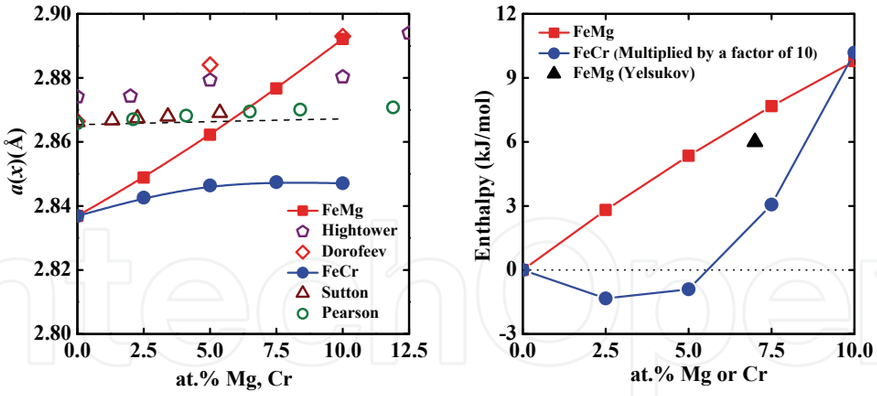

Fig. 1. Theoretical (EMTO, solid symbols connect with lines) lattice parameter (left panel) of ferromagnetic bcc Fe-Mg random alloys as a function of Mg concentration. The experimental data (open symbols) are from Ref. (Hightower et al., 1997) (Hightower) and Ref. (Dorofeev et al., 2004) (Dorofeev). For comparison, theoretical (EMTO) and available experimental Ref. (Sutton & Hume-Rothery, 1955)(Sutton) and Ref. (Pearson, 1958)(Pearson) lattice constant of ferromagnetic bcc Fe-Cr random alloys are also shown.The dashed line for Fe-Cr is obtained from Vegard's rule. Theoretical (EMTO) enthalpy of formation (right panel) for ferromagnetic bcc Fe-Mg random alloy. For comparison, the enthalpy of formation for Fe-Cr is also shown. The latter has been multiplied by 10 to match the scale. The predicted value by Yelsukov *et al.* (Yelsukov et al., 2005) for $Fe_{0.93}Mg_{0.07}$ is shown by triangle.

$\sim 0.5 \times 10^{-3}$ Å per at.% Cr (Pearson, 1958), but is in perfect agreement with the former *ab initio* calculation based on special quasi random structures (Olsson et al., 2006).

For the atomic radius of hcp Mg we obtained 1.764 Å, which agrees well with the experimental value of 1.77 Å (Young, 1991). Using this atomic radius and that of pure Fe (1.40 Å), for the bcc $Fe_{1-x}Mg_x$ alloys Vegard's rule predicts a lattice parameter with slope of $\Delta a(x)/\Delta x \sim 3.6 \times 10^{-3}$ Å per at.% Mg. The present EMTO results, shown in Fig. 1 (left panel), give 5.5×10^{-3} Å increase per at.% Mg. Moderate lattice expansion upon Mg addition to Fe was also reported by Hightower *et al.* (Hightower et al., 1997) and Dorofeev *et al.* (Dorofeev et al., 2004). In their measurements, the average lattice expansion below $x = 0.1$ was 0.6×10^{-3} and 2.7×10^{-3} Å per at.% Mg, respectively. Thus, similar to Fe-Cr, the present theoretical $\Delta a(x)/\Delta x$ seems to overestimate its experimental counterparts. On the other hand, the local experimental slope between 10 and 12.5 at.% Mg by Hightower *et al.* reaches 5.4×10^{-3} Å per at.% Mg, which is very close to the present value obtained for random solid solution. Surprisingly, our calculated density change of 11% obtained for $x = 0.1$ is in perfect agreement with the average experimental value measured below 10 at.% Mg (Fig. 1 in Ref.(Hightower et al., 1997)).

According to the experimental phase diagram, the solid solubility of Mg in Fe, and vice versa, is very small (Massalski, 1986), meaning that the formation energy of Fe-Mg alloy should be large and positive. In Fig. 1 (right panel) we compare the formation enthalpy of Fe-Mg with that of Fe-Cr. For the standard states, we use the ferromagnetic bcc Fe, the antiferromagnetic B2 Cr, and the experimental hexagonal closed packed (hcp) Mg with $c/a = 1.624$. The present enthalpy of formation for Fe-Cr shows a local negative minimum and becomes positive near 5.5% Cr, in good accordance with that reported in Refs. (Olsson et al., 2003; Korzhavyi et al., 2009).The enthalpy of formation for Fe-Mg, on the other hand, is found to increase monotonously up to 10 kJ/mol obtained for $Fe_{0.90}Mg_{0.10}$. This result is in line with the

predicted enthalpy of formation for Fe-Mg by de Boer *et al.* (de Boer et al., 1988) and also with that calculated by Yelsukov *et al.* (Yelsukov et al., 2005) for $Fe_{0.93}Mg_{0.07}$.

3.2 Single crystal elastic constants

For each Mg concentration x,the elastic constants were calculated at the corresponding theoretical equilibrium lattice parameter $a(x)$. The present theoretical single-crystal elastic constants $C_{ij}(x)$ of ferromagnetic bcc $Fe_{1-x}Mg_x$ ($0 \leq x \leq 0.1$) random alloys are plotted in Fig. 2 as a function of Mg content. We find that all elastic constants decrease nearly linearly with Mg addition. The theoretical $C_{11}(x), C_{12}(x), C'(x)$, and $C_{44}(x)$ for $x = 0.1$ change by about $-36.3\%, -34.2\%, -38.2\%$, and -8.2%, respectively, compared to the corresponding values for pure Fe. The monotonously decreasing trends of the $C_{ij}(x)$ of Fe-Mg (Fig. 2) indicating the absence of electronic topological transition in Fe-rich Fe-Mg random solid solutions.

Before turning to the polycrystalline elastic moduli, we discuss the effect of local lattice relaxation (LLR) around the impurity atoms on the single-crystal elastic constants. The LLR effect, neglected in the CPA calculations, is expected to become important in systems with large volume mismatch. Here we use a supercell technique to establish the order of magnitude of the effect of LLR on the C' elastic constant of Fe-Mg and Fe-Cr solid solutions. The 2x2x2 bcc supercell contained one Mg (or Cr) atom and 15 Fe atoms. First we calculated the tetragonal elastic constant of $Fe_{15}Mg_1$ ($Fe_{15}Cr_1$) using ideal bcc underlying lattice with lattice constant fixed to that obtained in a CPA calculation performed for the bcc $Fe_{0.9375}Mg_{0.0625}$ ($Fe_{0.9375}Cr_{0.0625}$) random alloy. Next we relaxed the first 8 nearest neighbor (NN) Fe atoms around the impurity atom and recalculated C' for the relaxed structure. In these calculations, we used ~ 2500 uniformly distributed k-points in the irreducible wedge of the Brillouin zone. Results from the supercell calculations are summarized in Table 1. We find that in $Fe_{15}Mg_1$ the equilibrium Fe-Mg distance is $\sim 0.8\%$ larger than the equilibrium Fe-Fe bond length in pure bcc Fe. This figure may be contrasted with $\sim 0.1\%$ contraction of the Fe-Cr distance in the Fe-Cr system relative to the Fe-Fe bond length. Comparing the tetragonal elastic constant calculated for the supercell having the ideal bcc structure (C'_u) to that calculated for the supercell with relaxed Fe-impurity distance (C'_r), we can estimate the LLR effect in C'. In $Fe_{15}Mg_1$ this effect is ~ 0.7 GPa and in $Fe_{15}Cr_1$ ~ 0.2 GPa. Since the alloying effects for both systems are significantly larger than the above LLR effects (Fig. 2), we conclude that the composition dependence of the elastic parameters of Fe-Mg and Fe-Cr systems is well captured by the present EMTO-CPA approach.

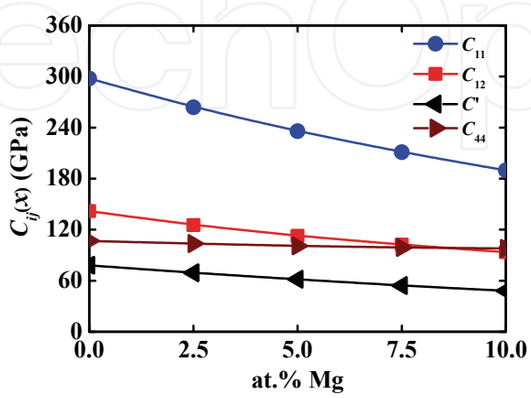

Fig. 2. Theoretical (EMTO) single-crystal elastic properties of ferromagnetic bcc Fe-Mg random alloys as a function of Mg concentration.

system	C'_u	δ_{NN}	C'_r
$Fe_{15}Mg_1$	56.61	0.8 %	57.33
$Fe_{15}Cr_1$	77.40	-0.1 %	77.57

Table 1. Results of the supercell calculations for $Fe_{15}Mg_1$ and $Fe_{15}Cr_1$ systems. δ_{NN} is the relaxation of the first nearest neighbor Fe atoms around the impurity atom. C'_u and C'_r (in GPa) are the tetragonal elastic constants obtained for the supercells without and with local lattice relaxation, respectively.

3.3 Polycrystalline elastic constants

The theoretical polycrystalline elastic moduli for ferromagnetic bcc $Fe_{1-x}Mg_x$ ($0 \leq x \leq 0.1$) random alloys are displayed as a function of Mg content in Fig. 3. Similar to the single-crystal elastic constants (Fig. 2), the polycrystalline elastic moduli also decrease with Mg content. These results could in fact be anticipated if, for instance, we take into account that the theoretical bulk modulus of hcp Mg is significantly smaller than that of bcc Fe. However, the actual slope of B in Fig. 3 is much larger than that predicted from the ~ 157 GPa difference between the theoretical bulk moduli of Fe and Mg by assuming a linear composition dependence for $B(x)$. We find that for $x = 0.1$, $B(x), G(x), E(x)$, and $B/G(x)$ decrease by about 35.2%,21.7%,23.9%, and 17.3%, respectively, relative to those of pure Fe. Above 7.5 at.% Mg, the calculated $B/G(x)$ ratio of Fe-Mg alloys drops below the brittle-ductile limit of 1.75 set by Pugh (Pugh, 1954), implying that Mg addition makes the ferromagnetic bcc Fe-Mg alloys brittle.

The theoretical Poisson's ratio ($\nu(x)$) and Debye temperature ($\Theta(x)$) of Fe-Mg are shown in Fig. 4, for comparison theoretical and experimental (Speich et al., 1972) Poisson's ratio and Debye temperature of Fe-Cr are also shown. For Fe-Cr, the Poisson's ratio slightly decreases with Cr concentration up to 10 at.% Cr, in line with the experimental data (Speich et al., 1972). The Debye temperature exhibits a monotonous enhancement with Cr content. In $Fe_{0.9}Cr_{0.1}$, the calculated Poisson's ratio decreases by 9.97% and the Debye temperature enhances by 4.45% with respect to that for pure Fe.

For Fe-Mg, both of them exhibit a nearly linear decreasing dependence on the chemical

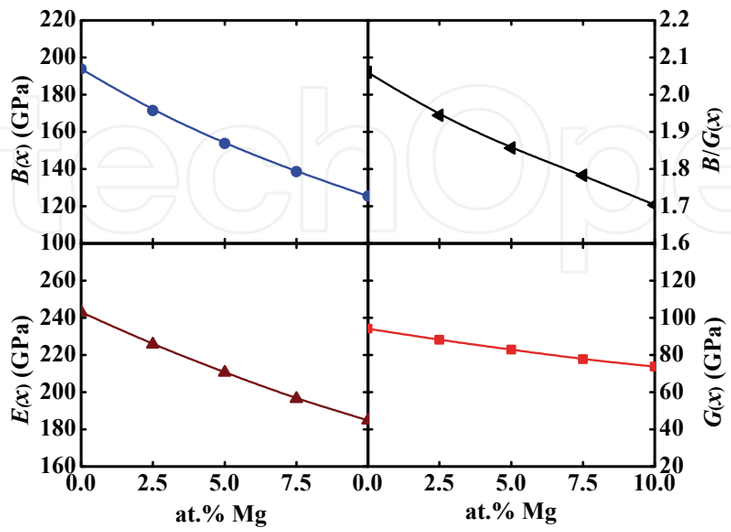

Fig. 3. Theoretical (EMTO) polycrystalline elastic properties of ferromagnetic bcc $Fe_{1-x}Mg_x$ ($0 \leq x \leq 0.1$) random alloys as a function of Mg concentration.

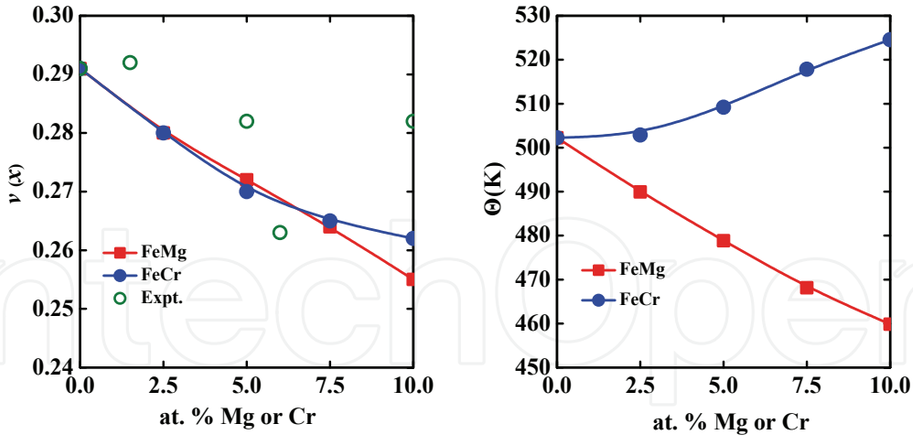

Fig. 4. Theoretical (EMTO) Poisson's ratio (left panel) and Debye temperature (right panel) of ferromagnetic bcc $Fe_{1-x}Mg_x$ ($0 \leq x \leq 0.1$) random alloys as a function of Mg concentration. For comparison, theoretical and experimental (Speich et al., 1972)Poison's ratio and Debye temperature for Fe-Cr are also shown.

composition. At 10 at.% Mg, the Poisson's ratio and Debye temperature are by 12.37% and 8.45%, respectively, smaller than those corresponding to pure Fe. This Debye temperature drop when going from Fe to $Fe_{0.90}Mg_{0.1}$ is expected to give a phonon vibration energy contribution which stabilizes the solid solution. To estimate this effect, we make use of the high-temperature expansion of the phonon energy (Grimvall, 1976). Namely, for two solids with similar Debye temperatures, the vibrational free energy difference is $\Delta F^{\rm vib} \approx 3k_{\rm B}T(\Delta\Theta/\Theta)$, where T is the temperature, $\Delta\Theta/\Theta$ is the relative Debye temperature and $k_{\rm B}$ the Boltzmann constant. We write the phonon free energy of formation for $Fe_{1-x}Mg_x$ as $\Delta F^{\rm vib}(x) = x\left[F^{\rm vib}(x) - F^{\rm vib}({\rm Mg})\right] + (1-x)\left[F^{\rm vib}(x) - F^{\rm vib}({\rm Fe})\right]$, where $F^{\rm vib}(x)$, $F^{\rm vib}({\rm Mg})$, and $F^{\rm vib}({\rm Fe})$ are the vibrational free energies for $Fe_{1-x}Mg_x$, Mg, and Fe, respectively. For $x = 0.1$ we have $\left[\Theta(0.1) - \Theta({\rm Fe})\right]/\Theta({\rm Fe}) \approx -0.0845$ and $\left[\Theta(0.1) - \Theta({\rm Mg})\right]/\Theta({\rm Mg}) \approx 0.406$, where for the Debye temperature of Mg we used 327 K (Grimvall, 1999). Using these relative Debye temperatures, we arrive at $\Delta F^{\rm vib}(0.1) \approx -0.884 \times 10^{-3} T$ kJ/mol/K (referring to mole of atoms). For comparison, the configuration entropy for $Fe_{0.90}Mg_{0.1}$, evaluated within the mean-field approximations, is $\Delta F^{\rm conf}(0.1) \approx -2.70 \times 10^{-3} T$ kJ/mol/K. It is worth noting that according to Fig. 1 (right panel), the total thermal free energy $\Delta\left[F^{\rm vib}(0.1) + F^{\rm conf}(0.1)\right] = -3.584 \times 10^{-3} T$ kJ/mol/K would stabilize the random $Fe_{0.90}Mg_{0.1}$ solid solution at ~ 2790 K, *i.e.* above the melting point of Fe.

4. Iron-magnesium alloys at Earth's core conditions

In this chapter we review the thermo-physical properties of hexagonal closed-packed and body-centered cubic iron-magnesium alloys at high pressure (and high temperature), up to the conditions of the Earth's solid inner core. We discuss the relevance of the theoretical results to the inner core.

4.1 Hexagonal closed-packed iron-magnesium alloys

In the following, we demonstrate the elastic properties of hexagonal closed-packed iron-magnesium alloys at high pressures and zero temperature (Kádas et al., 2008a).

Volume	C_{11}	C_{33}	C_{12}	C_{13}	C_{44}	
51.0	1545.5	1760.8	709.1	540.3	346.7	present work
49.6	1533.0	1544.0	846.0	835.0	583.0	Expt.[a]
50.0	1675	1835	735	645	415	LAPW[b]
49.9	1625.0	1867.6	809.3	639.2	356.5	APW+lo[c]
50.9	1510	1450	460	673	414	FP-LMTO[d]

[a] Ref. Mao et al. (1998)
[b] Ref. Steinle-Neumann et al. (1999)
[c] Ref. Qiu & Marcus (2003)
[d] Ref. Söderlind et al. (1996)

Table 2. Theoretical and experimental elastic constants (in GPa) of nonmagnetic hcp Fe at $\sim$50 Bohr^3/atom. All the theoretical results were obtained at zero temperature, while measurements were performed at room temperature.

In order to check the accuracy of our method, we compare the present results obtained for pure nonmagnetic hcp Fe to the available experimental and ab initio theoretical data at V=$\sim$50 Bohr^3/atom volume (Table 2).
We obtain a reasonable agreement both with theoretical and experimental results. The present theoretical values agree with the full-potential linearized-augmented plane-wave (LAPW, (Steinle-Neumann et al., 1999)), full-potential augmented plane-wave plus local orbital (APW+lo, (Qiu & Marcus, 2003)) and full-potential linear muffin-tin orbitals (FP-LMTO, (Söderlind et al., 1996)) results within $\sim$20%, except C_{12}, where the FP-LMTO method provides significantly smaller value than the other ab initio methods. We find larger deviations from the X-ray diffraction measurements (Mao et al., 1998) for C_{13} and C_{44}, where the experiment provides notably larger values than any theoretical methods, even if we take into account that the experimental volume is a little bit smaller than any of the theoretical ones.

4.1.1 Equation of state

Prior to the calculation of the equation of state, we need to optimize the hexagonal axial ratio, c/a, at each V volume for pure Fe and hcp Fe-Mg alloys. Panel (a) in Fig. 5 shows that c/a increases with increasing pressure for pure Fe and Fe-Mg alloys (Kádas et al., 2008a). However, the change in c/a is rather small, in the whole studied pressure range, it increases by 0.7%, 0.6% and 0.5% in pure Fe, $Fe_{0.95}Mg_{0.05}$ and $Fe_{0.9}Mg_{0.1}$, respectively. We obtain the lowest c/a values for pure Fe, and find that c/a increases with Mg content. Compared to pure Fe, the average change in c/a is 0.3% in $Fe_{0.95}Mg_{0.05}$, and 0.6% in $Fe_{0.9}Mg_{0.1}$. We note that the experimental c/a values for pure iron in the 34.8-300.6 GPa pressure range (Mao et al., 1990) are very scattered and they vary between 1.575 and 1.602.
The theoretical equation of state is shown in Fig. 5 (b). At any pressure, the volume increases with increasing Mg content compared to pure iron. This can be explained with the larger atomic size of Mg: its metallic atomic radius is 27% larger than that of Fe. As the pressure increases, the change in volume with increasing Mg concentration decreases, which can be understood by considering that Mg has a much higher compressibility, than Fe (Dubrovinskaia et al., 2005).

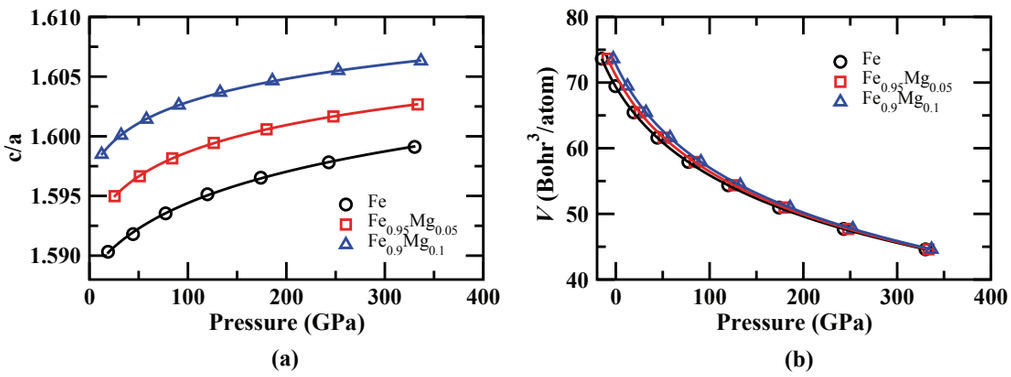

Fig. 5. Theoretical pressure dependency of the hexagonal axial ratios (c/a) and the volume of pure hcp Fe (circles), $Fe_{0.95}Mg_{0.05}$ (squares) and $Fe_{0.9}Mg_{0.1}$ (triangles).

4.1.2 Single crystal elastic constants

The theoretical elastic constants of Fe, $Fe_{0.95}Mg_{0.05}$ and $Fe_{0.9}Mg_{0.1}$ at different volumes are shown in Table 3.

All the elastic constants follow a normal decreasing behavior with increasing volume. Their average changes in this volume interval are ΔC_{11}=-70%, ΔC_{33}= -69%, ΔC_{12}=-77%, ΔC_{13}=-79% and ΔC_{44}=-62%. We observe monotonous change with the Mg concentration at each volume: C_{11}, C_{33} and C_{44} decrease with increasing Mg content, while C_{12} and C_{13} slightly increase. $C_{66} = (C_{11} - C_{12})/2$ decreases with increasing Mg concentration. We calculate the largest variations for C_{44}: compared to pure iron, it decreases by 14% in $Fe_{0.95}Mg_{0.05}$ and 27% in $Fe_{0.9}Mg_{0.1}$ at V=44.6 Bohr^3/atom. Both pure hcp Fe and Fe-Mg alloys are mechanically stable in the whole pressure range considering the following stability criteria (Grimvall, 1999), $C_{11} > |C_{12}|$, $C_{33}(C_{11} + C_{12}) > 2C_{13}^2$, $C_{11}C_{33} > C_{13}^2$ and $C_{44} > 0$, which are fulfilled at any volume and Mg content.

Volume	C_{11}	C_{33}	C_{12}	C_{13}	C_{44}
		Fe:			
44.602	2257.1	2597.4	1151.2	873.3	476.6
50.965	1545.5	1760.8	709.1	540.3	346.7
65.450	676.8	773.9	240.5	179.2	178.8
		$Fe_{0.95}Mg_{0.05}$:			
44.602	2159.2	2503.2	1169.1	869.6	411.6
50.965	1476.3	1707.6	739.3	544.6	303.9
65.450	653.4	767.9	264.3	187.6	157.4
		$Fe_{0.9}Mg_{0.1}$:			
44.602	2036.5	2398.7	1206.2	875.7	348.5
50.965	1399.3	1650.5	775.7	552.9	261.2
65.450	633.1	752.0	289.9	196.1	136.6

Table 3. Theoretical elastic constants (in GPa) of hcp Fe and hcp Fe-Mg alloys at different volumes (in Bohr^3/atom). These volumes correspond to pressures between approximately 18 and 340 GPa.

4.1.3 Polycrystalline elastic constants

In the following, we examine the effect of Mg alloying on the physical properties of iron, and compare our theoretical results to those of the PREM model. Panel (a) in Fig. 6 shows that Mg decreases the bulk modulus, B, at any pressure. We find that B of the $Fe_{0.9}Mg_{0.1}$ alloy is in an excellent agreement with PREM data of the inner core. We note, however, that our calculations were performed at zero temperature, and according to the theoretical results of Steinle-Neumann et al., B increases in Fe with increasing temperature (Steinle-Neumann et al., 2001).

Examining the effect of alloying on the density, we find that the increasing Mg concentration decreases it at any given pressure (Fig. 6 (b)). However, the densities of Fe-Mg alloys do not reach those of the inner core reported in the PREM model, not even at 10% Mg content. The shear modulus decreases with increasing Mg content (Fig. 6 (c)). Though at core pressures 10% Mg alloying reduces the shear modulus by 23%, compared to pure iron, it is still insufficient to reproduce shear moduli of the inner core. For the sound velocities, we find that the longitudinal (compressional) sound wave velocity, v_P, slightly decreases with increasing Mg alloying (Fig. 6 (d)), and even at 10% Mg concentration, we calculate about 20% larger values than those of the PREM values at the Earth's inner core. The transverse (shear) sound velocity, v_S, decreases to a larger extent with increasing Mg content than v_P. Although at core pressures 10% Mg alloying reduces v_S by 12%, compared to pure iron, we obtain here ∼45% larger values than those expected in the inner core. We note that both the

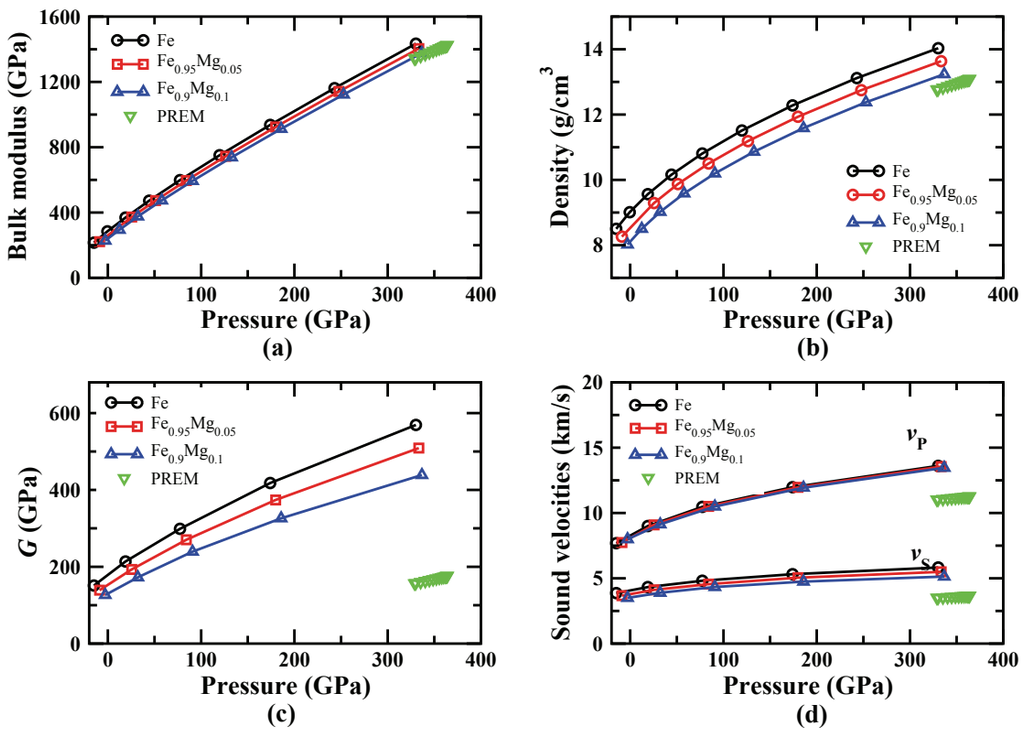

Fig. 6. Theoretical bulk modulus (a), density (b), shear modulus, G (c), and sound velocities (d) of pure hcp Fe (circles), $Fe_{0.95}Mg_{0.05}$ (squares) and $Fe_{0.9}Mg_{0.1}$ (triangles) as a function of pressure. v_P and v_S denote longitudinal and transverse sound velocities, respectively. Seismic data as given in the PREM model are shown for comparison (inverted triangles).

present calculated v_P and v_S values, being in linear relation with the density, fulfill Birch's law (Birch, 1961) at any Mg concentration.
In summary, investigating the elastic properties of iron-rich hcp Fe-Mg alloys, containing 5 and 10 atomic % Mg, up to pressures of the Earth's inner core, we found that in these systems the increasing Mg content decreases the bulk modulus, density and both the longitudinal and transverse sound velocities. Mg alloying changes the elastic properties of hcp iron in such a way that the differences to the PREM values decrease. Our results indicate that Mg should be considered as a possible component of the Earth's inner core. In addition, we note that agreement between the calculated value of the bulk modulus and that of PREM is not a sufficient test for a compositional model of the inner core, as has been noted in the literature before.

4.2 Body-centered cubic iron-magnesium alloys

I the following, we demonstrate the thermo-physical properties of body-centered cubic iron-magnesium alloys at high pressure and high temperature (Kádas, Vitos, Johansson & Ahuja, 2009).

4.2.1 Equation of state

We calculated the equation of state for pure bcc Fe, as well as for bcc $Fe_{1-x}Mg_x$ ($Fe_{0.95}Mg_{0.05}$ and $Fe_{0.9}Mg_{0.1}$) alloys at zero temperature (Fig. 7). For comparison, for pure Fe both the nonmagnetic (NM) and ferromagnetic (FM) states were considered. Figure 7 shows that the volumes of NM and FM bcc Fe are notably different at low pressure, but the volume difference gradually decreases with increasing pressure and disappears around ≈300 GPa. This is in line with the gradually vanishing calculated ferromagnetic moment on Fe. We also modelled the high temperature paramagnetic phase using the disordered local magnetic moment (DLM) approach. The DLM was proven to describe the effect of loss of the net magnetic moment accurately above the transition temperature (Oguchi et al., 1983). Our calculated DLM moments rapidly vanish with pressure and become zero already at ∼10 GPa. The effect of Mg-alloying can be observed in Fig. 7. At low pressures, the volume of Fe-Mg alloys increases with the Mg content, due to the larger atomic size of Mg. Since Mg has higher compressibility, than Fe, the change in volume with increasing Mg concentration decreases

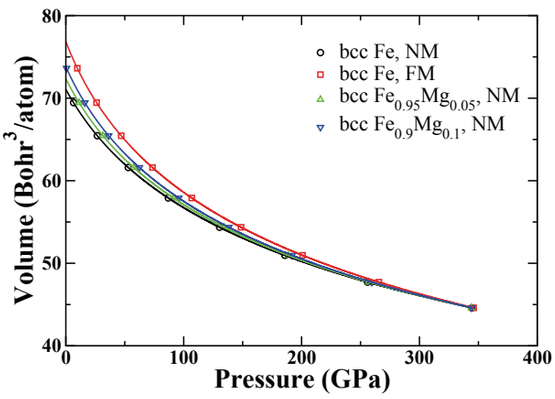

Fig. 7. Calculated equation of state for nonmagnetic (NM) and ferromagnetic (FM) pure bcc Fe (denoted by black circles and red squares, respectively), NM bcc $Fe_{0.95}Mg_{0.05}$ (red triangles), and bcc $Fe_{0.9}Mg_{0.1}$ alloys (blue inverted triangles).

with increasing pressure. The volume difference between pure Fe and Fe-Mg alloys practically vanishes at core pressures (329-364 GPa (Dziewonski & Anderson, 1981)).

4.2.2 Single crystal elastic constants

The zero temperature shear elastic constants, C', C_{44}, and the bulk modulus, B, calculated at different V volumes for for pure bcc Fe, $Fe_{0.95}Mg_{0.05}$ and $Fe_{0.9}Mg_{0.1}$ alloys are shown in Fig. 8 (solid lines). At T=0 K, pure bcc Fe is dynamically unstable, since one of its elastic constants, the tetragonal shear modulus (C') is negative at each volume. In addition, C' shows an anomalous behavior: it increases with increasing volume. However, C' remains negative at each volume, even in $Fe_{0.9}Mg_{0.1}$. We calculate $(\Delta C'/\Delta V)_{Fe}$=7.6 GPa/Bohr^3 for pure iron, and $(\Delta C'/\Delta V)_{Fe_{0.95}Mg_{0.05}}$=4.1 GPa/Bohr^3 and $(\Delta C'/\Delta V)_{Fe_{0.9}Mg_{0.1}}$=1.7 GPa/Bohr^3 for the alloys. C_{44} and B follow a normal decreasing behavior with increasing volume.

At T=7000 K, in our calculations, pure bcc Fe is still unstable at high pressures, i.e. at small volumes. Namely, at V=44.60 Bohr^3/atom, we calculate C'=-43.71 GPa for Fe at T=7000 K. We find that small amount of magnesium addition stabilizes dynamically the bcc phase of Fe-Mg alloys. At the lowest core temperature (∼5000 K), we obtain $C'(Fe_{0.91}Mg_{0.09})$=6.4 GPa at 355 GPa. However, at higher temperature, i.e. closer to the centre of the core, significantly less Mg is sufficient for dynamical stability. For instance, at 7000 K already 5 at.% Mg addition leads to positive C' for the bcc phase (Fig. 8). C_{44} and B decrease with increasing volume in both pure Fe and in Fe-Mg alloys at T=7000 K. The high temperature bulk moduli are slightly larger than those calculated at zero temperature (Fig. 8).

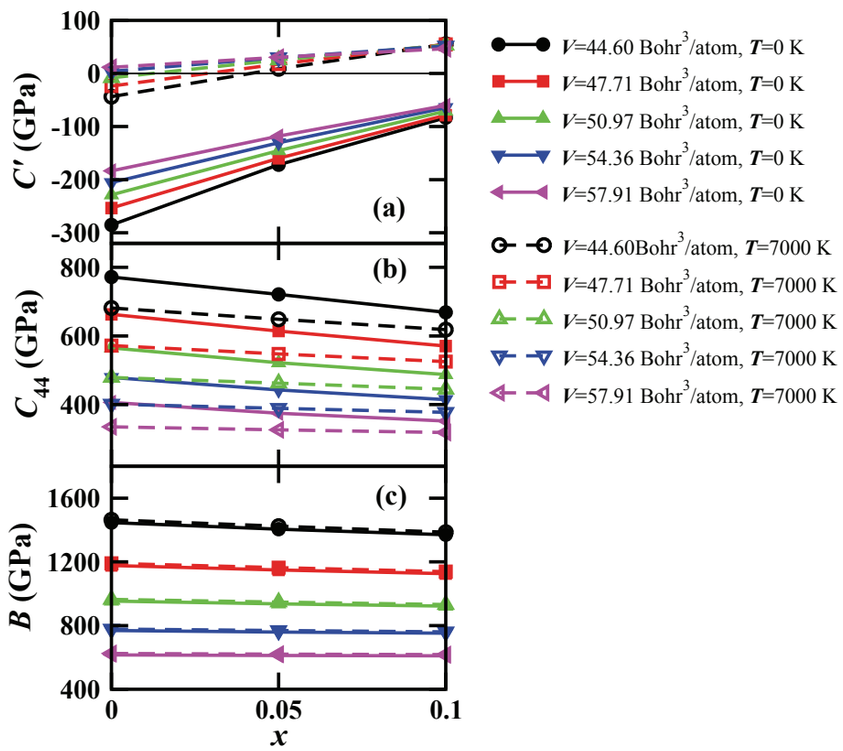

Fig. 8. Single crystal elastic constants, C', C_{44}, and the bulk modulus, B, as a function of Mg concentration, x, calculated at different V volumes at zero temperature (solid lines) and at T=7000 K (dashed lines). The horizontal black line in panel (a) corresponds to C'=0 GPa.

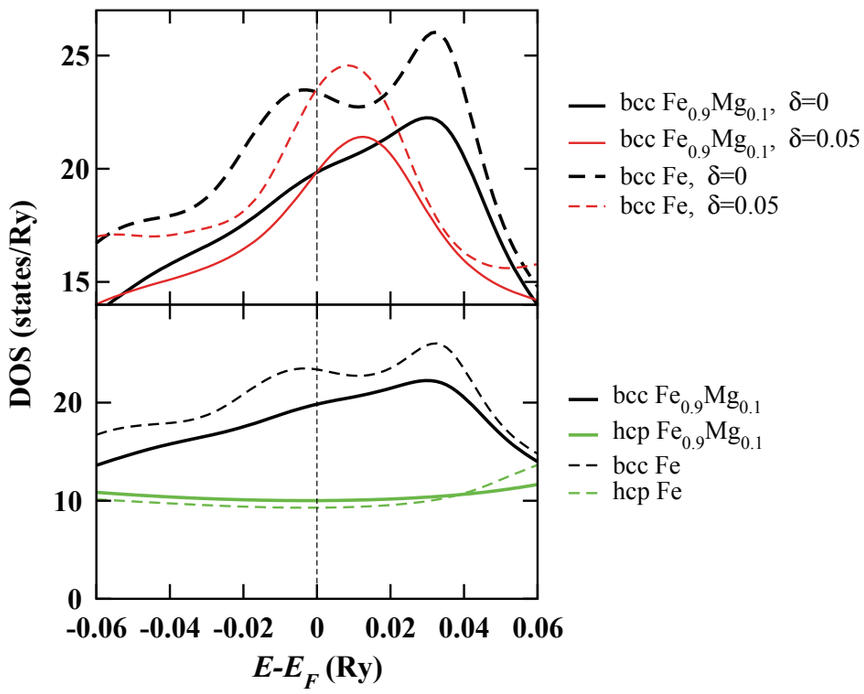

Fig. 9. Electronic density of states of Fe at T=0 K for an energy window corresponding to ~5000-8000 K. Lower panel: density of states of Fe and $Fe_{0.9}Mg_{0.1}$ in the bcc and hcp phases, respectively. Upper panel: density of states for non-distorted bcc Fe and $Fe_{0.9}Mg_{0.1}$ (δ=0) and for distorted bcc Fe and $Fe_{0.9}Mg_{0.1}$ (δ=0.05). Similar orthorhombic distortions have been used to compute the tetragonal cubic shear modulus C'. Vertical dashed lines denote the Fermi level.

To understand the role of Mg on the dynamical stability of the bcc phase, we follow the effect of the orthorhombic distortion δ (used to compute C') on the bcc DOS (Fig. 9, upper panel). In bcc Fe, the orthorhombic distortion splits the degenerated *d* peak located around -7 mRy below E_F (corresponding mainly to the e_g states), pushing one *d* band towards negative energies and one *d* band above the Fermi level. Because of that, the DOS between -40 mRy and E_F decreases, which gives a substantial negative contribution to the electronic energy. Consequently, the total energy decreases upon lattice distortion yielding a large negative tetragonal shear constant for bcc Fe (C'_{Fe}=-285 GPa at 0 K and 44.6 $Bohr^3$/atom). This mechanism is responsible for the dynamical instability of bcc Fe at core pressures and low temperatures. In Fe-Mg alloys, the above effect is greatly diminished. Due to the chemical disorder, the DOS is much smoother near the Fermi level in $Fe_{0.9}Mg_{0.1}$ compared to that in pure Fe (Fig. 9, upper panel, black solid line). As a result, the energy decrease upon lattice distortion is less dominant for the alloy than for pure Fe. This leads to a significantly larger C' for Fe-Mg than for Fe already at low temperatures ($C'_{Fe_{0.9}Mg_{0.1}}$=-83 GPa at 0 K and 44.6 $Bohr^3$/atom).

The marked difference between the bcc and hcp DOS's near E_F (Fig. 9) is also reflected in the temperature effects. The electron excitations are more significant in the case of the bcc structure than for the hcp structure. This is because, first the DOS at E_F is notably larger in the bcc phase, and second the DOS at E_F is very irregular in the bcc phase in contrast to the almost

constant DOS in the hcp phase. The increasing temperature increases C' of bcc Fe, because of the strong increase in the electronic entropy with distortion. This gives positive contribution to the Gibbs free energy. In pure Fe at 6000 K, the electronic entropy term in the Gibbs free energy (-TS_e) is increased by 3.1 mRy with orthorhombic distortion, compared to that of the non-distorted system. In $Fe_{0.9}Mg_{0.1}$, -TS_e is increased by 1.7 mRy in the distorted structure, which indicates that the dynamical stabilization effect of temperature is larger in pure Fe than in Fe-Mg alloys. However, this can not compensate the large chemical stabilization effect of Mg present already at low temperatures. Accordingly, we calculate C'(Fe)=-77 GPa and $C'(Fe_{0.9}Mg_{0.1})$=37.0 GPa at 6000 K and 44.6 Bohr^3/atom (356 GPa).

4.2.3 Polycrystalline elastic constants

The polycrystalline shear modulus (G) can not be defined for dynamically unstable systems. Accordingly, in the following, we examine the polycrystalline elastic constants at T=7000 K temperature, for the dynamically stable bcc Fe-Mg alloys, and reveal the effect of Mg alloying on the elastic properties. The Hashin-Shtrikman averages (Hashin & Shtrikman, 1962) of the shear modulus (G), the Young modulus (E), the polycrystalline anisotropy (A), and the longitudinal (v_P) and transversal (v_S) sound velocities calculated for bcc $Fe_{0.95}Mg_{0.05}$ and $Fe_{0.9}Mg_{0.1}$ alloys at different volumes and at T=7000 K are shown in Fig. 10. The shear modulus follows a normal decreasing behavior with increasing volume in both alloys (Fig. 10, panel (a)). Between V=44.60 and V=57.91 Bohr^3/atom G decreases by 20% in $Fe_{0.95}Mg_{0.05}$, and 39% in $Fe_{0.9}Mg_{0.1}$. The shear modulus increases with Mg alloying at each volume considered here. The change in G, due to the increased Mg content, diminishes with increasing volume. This is because G decreases almost linearly with increasing volume in $Fe_{0.9}Mg_{0.1}$, while in $Fe_{0.95}Mg_{0.05}$ $|\Delta G/\Delta V|$ increases with increasing volume. G is 49% larger in $Fe_{0.9}Mg_{0.1}$ than in $Fe_{0.95}Mg_{0.05}$ at V=44.60 Bohr^3/atom, and the corresponding difference in G is only 15% at V=57.91 Bohr^3/atom.

Magnesium enhances the stiffness of bcc Fe at T=7000 K, as the Young moduli, $E = 9BG/(3B + G)$, are higher in $Fe_{0.9}Mg_{0.1}$ than in $Fe_{0.95}Mg_{0.05}$ at each volume (panel (b) in Fig. 10). In $Fe_{0.9}Mg_{0.1}$, E decreases approximately linearly with increasing volume (i.e. with decreasing pressure), while in $Fe_{0.95}Mg_{0.05}$ $|\Delta E/\Delta V|$ increases with increasing volume. Because of this, the change in E due to 5% Mg addition diminishes with increasing volume: E is 47% larger in $Fe_{0.9}Mg_{0.1}$ than in $Fe_{0.95}Mg_{0.05}$ at V=44.60 Bohr^3/atom, and this difference is reduced to 14% at V=57.91 Bohr^3/atom.

In polycrystalline materials,

$$A = \frac{G_V - G_R}{G_V + G_R} \tag{13}$$

can be used as a measure of elastic anisotropy, where G_V and G_R are the Voigt and Reuss shear moduli (Grimvall, 1999). In an isotropic material, the Voigt and Reuss averages of the shear moduli are equal, so that A=0. The more anisotropic a material is, the larger A value it has. The bcc Fe-Mg alloys considered here are highly anisotropic: A varies between 0.90 and 0.51 in $Fe_{0.95}Mg_{0.05}$, and it changes between 0.53 and 0.37 in $Fe_{0.9}Mg_{0.1}$. The anisotropy is larger in $Fe_{0.95}Mg_{0.05}$ than in $Fe_{0.9}Mg_{0.1}$ at each volume (Fig. 10, panel (c)), indicating that the increasing Mg content decreases the anisotropy of the alloys. For both alloys the anisotropy decreases with increasing volume. As a comparison, we note, that there is a significant difference in anisotropy between the two phases, namely the bcc and hcp phases of pure Fe. Hexagonal Fe is almost isotropic: A=0.02 at V=44.60 Bohr^3/atom (Kádas et al.,

2008a). In this phase, Mg alloying does not change anisotropy notably: at the same V=44.60 Bohr^3/atom volume, A=0.03 in hcp $Fe_{0.95}Mg_{0.05}$, and A=0.04 in hcp $Fe_{0.9}Mg_{0.1}$.

The longitudinal sound velocity can be calculated as $v_P = \sqrt{\frac{B+4G/3}{\varrho}}$, where ϱ is the density. The longitudinal sound velocity decreases linearly with increasing volume (panel (d) in Fig. 10) in both $Fe_{0.95}Mg_{0.05}$ and $Fe_{0.9}Mg_{0.1}$. Since $B \gg G$ in these alloys, we find that $v_P \sim \sqrt{B}$, which in turn follows a linear trend with volume. Increasing Mg content raises v_P at each V volume.

The transversal sound velocity, $v_S = \sqrt{G/\varrho}$, monotonically decreases with increasing volume in $Fe_{0.9}Mg_{0.1}$ (panel (e) in Fig. 10). In $Fe_{0.95}Mg_{0.05}$, v_S follows a different behavior: it increases with increasing volume up to V=50.97 Bohr^3/atom, and decreases above V=54.36 Bohr^3/atom. The trend in v_S vs. volume obtained for $Fe_{0.95}Mg_{0.05}$ and $Fe_{0.9}Mg_{0.1}$ can be explained by v_S being approximately proportional to $\sqrt{G}$ in bcc Fe-Mg alloys. The transversal sound velocity is raised by increasing Mg content at each volume.

4.3 Implications for the Earth's inner core

Iron-based alloys at high pressure and temperature are relevant to the Earth's solid inner core. There are extreme conditions in this part of our planet: the pressure varies between 329 and 364 GPa (Dziewonski & Anderson, 1981), and the temperature changes between 5000 and 8000 K (Hemley & Mao, 2001).

We showed in Section 4.1.3 that Mg alloying changes the elastic properties of hcp iron in such a way that the differences to the PREM values decrease. However, the shear modulus and both the longitudinal and transversal sound velocities significantly differ from those

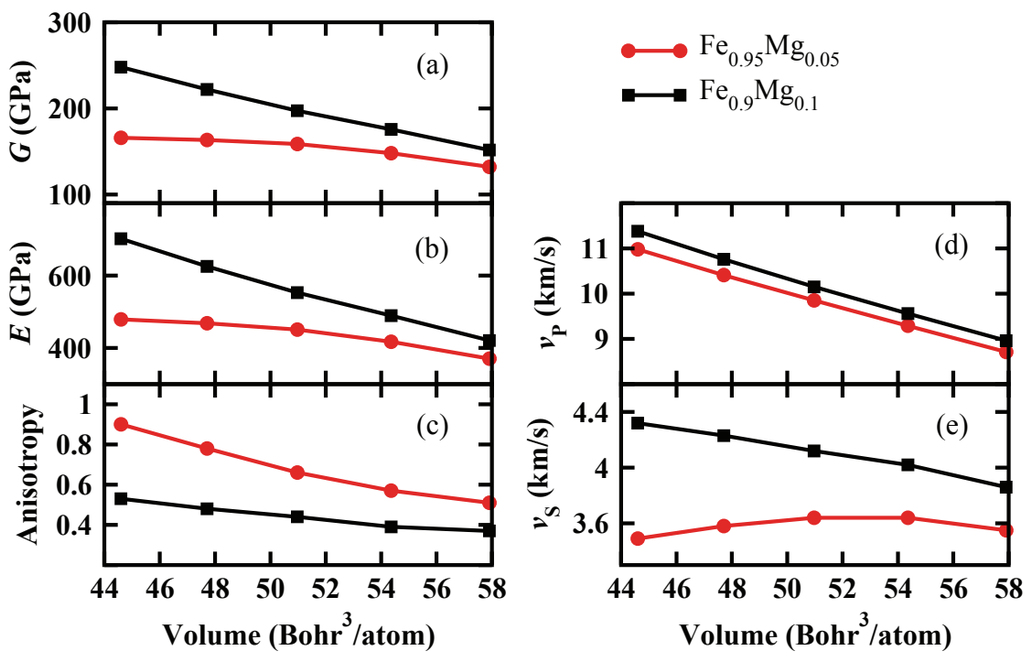

Fig. 10. Shear (G) and Young moduli (E), polycrystalline anisotropy, and longitudinal (v_P) and transversal (v_S) sound velocities of bcc $Fe_{0.95}Mg_{0.05}$ (red circles) and $Fe_{0.9}Mg_{0.1}$ alloys (black squares) at different V volumes, at T=7000 K temperature.

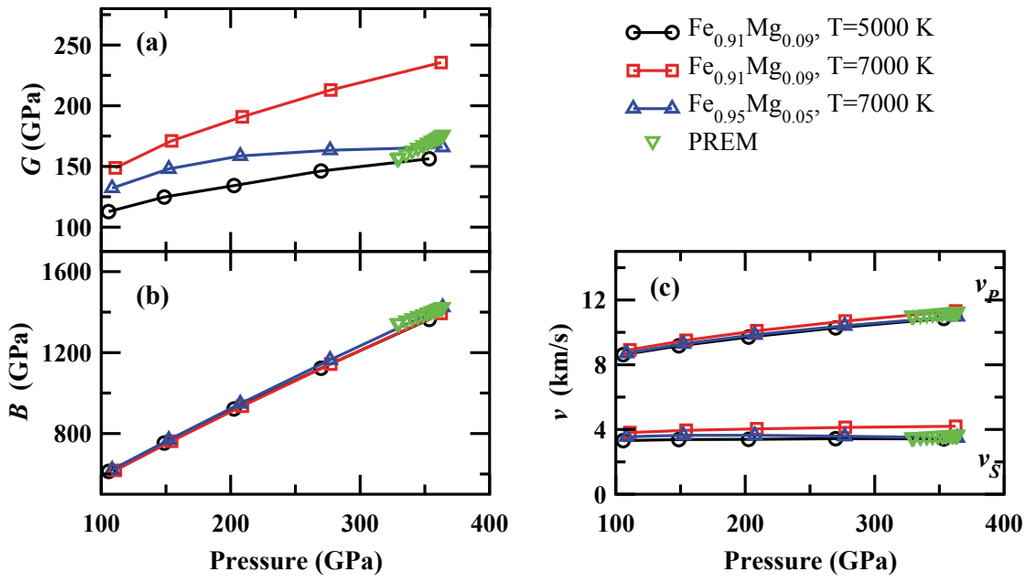

Fig. 11. Shear and bulk moduli, and sound velocities of bcc Fe-Mg alloys. Calculated shear moduli (a), bulk moduli (b) and sound velocities (v_S shear wave and v_P compressional wave velocities, panel (c)) are displayed for $Fe_{0.91}Mg_{0.09}$ at temperatures of T=5000 K (circles) and T=7000 K (squares), and for $Fe_{0.95}Mg_{0.05}$ at T=7000 K (triangles). Seismic data as given in the PREM model (Dziewonski & Anderson, 1981) are shown for comparison (inverted triangles).

of the PREM values at the Earth's inner core. The electronic DOS of hcp Fe (Fig. 9) indicates that the electronic excitations are not as significant in the hcp phase of Fe than in the bcc phase. Therefore we do not expect dramatic changes in the elastic constants at high temperature, compared to zero temperature. Accordingly, one may not expect significantly better agreement in the shear modulus and sound velocities of hcp Fe-Mg alloys with PREM data at high temperature than at T=0 K.

Therefore, in the following we focus on bcc-structured alloys, and we compare the theoretical high-temperature elastic properties of bcc Fe-Mg alloys with seismic data of the inner core, as given in the PREM model (Dziewonski & Anderson, 1981).

The calculated density of the bcc $Fe_{0.91}Mg_{0.09}$ alloy is 13.17 g/cm^3 at 5000 K and 350 GPa, which shows an excellent agreement with the corresponding core density (Dziewonski & Anderson, 1981), the deviation being 1.6%. The present density is smaller than 13.58 g/cm^3 obtained from ab initio molecular dynamics simulations (Belonoshko et al., 2007) for pure bcc iron at 356.7 GPa. In Fig. 11, we compare the shear (G) and bulk (B) moduli, as well as compressional (v_P) and shear (v_S) wave velocities of $Fe_{0.91}Mg_{0.09}$ at 5000 and 7000 K, and those of $Fe_{0.95}Mg_{0.05}$ at 7000 K with the PREM data. The shear modulus of $Fe_{0.91}Mg_{0.09}$ at 5000 K is in very good agreement with the seismic data, the deviation being -7.8% at 353 GPa (panel (a)). The figure also demonstrates that G increases with increasing temperature at constant Mg content. However, at higher temperatures smaller amount of Mg can stabilize bcc Fe, and G sensitively decreases with decreasing Mg concentration. Accordingly, $G(Fe_{0.95}Mg_{0.05})$ at 7000 K agrees excellently with those of the core: the present theoretical value at 363 GPa differs by -5.8% from the seismic data. The calculated bulk moduli (Fig. 11 (b)) are also very close to those of the inner core (Dziewonski & Anderson, 1981). $B(Fe_{0.91}Mg_{0.09})$ differs from the seismic data by -2.5% and -2.1% at 5000 and 7000 K, respectively, while the deviation

for $Fe_{0.95}Mg_{0.05}$ at 7000 K is only -0.1%. The compressional (P-wave) velocity also shows an excellent agreement with PREM (Fig. 11 (c)). At core pressures, the deviations between theoretical and PREM v_P values are -2.9% and 0.6% for $Fe_{0.91}Mg_{0.09}$ at 5000 K and 7000 K, respectively, and -2.5% for $Fe_{0.95}Mg_{0.05}$ at 7000 K. It has been shown (Vočadlo, 2007) that both bcc and hcp phases of pure Fe, as well as FeS and FeSi have significantly higher shear wave velocities than those deduced from seismology. At the same time, the present theoretical shear wave velocity (Fig. 11 (c)) agrees well with PREM for $Fe_{0.91}Mg_{0.09}$ at 5000 K: the difference being -5.4% at 353 GPa. At 7000 K and 362 GPa, the deviation between theoretical and PREM v_S values is somewhat larger (14.6%). However, v_S decreases with decreasing Mg content, and we obtain an excellent agreement (-4.8%) with seismic data for $Fe_{0.95}Mg_{0.05}$ at 7000 K and 363.8 GPa.
In summary, a bcc-structured Fe-Mg alloy containing 5-10% Mg in fact reproduces the physical properties of the Earth's inner core, as given in the PREM model, which makes it a very strong candidate structural model for the core.

5. Conclusions

Using the EMTO method in combination with the coherent-potential approximation, we have calculated the single-crystal and polycrystalline elastic properties of ferromagnetic bcc Fe-Mg random alloys encompassing up to 10 at.% Mg. At ambient conditions, all elastic parameters of ferromagnetic bcc Fe-Mg decrease in an almost linear manner with Mg addition. In general, Mg is found to have a more pronounced impact on the elastic properties of Fe-based alloys than that of Cr. In particular, the B/G ratio decreases by 17.3% when 10% Mg is added to bcc Fe, indicating that Mg reduces the ductility of Fe. According to the classical solid-solution strengthening models (Vitos & Johansson, 2007; Labusch, 1972), the large alloying effects obtained for the Fe-Mg alloys should result in an enhanced mechanical hardness. These predictions are subject for further theoretical investigations and call for well designed experimental studies on the mechanical properties of Fe-rich Fe-Mg solid solutions. We showed that at Earth's core pressures, Mg alloying changes the elastic properties of hcp iron in such a way that the differences to the seismic data decrease. The calculated shear moduli and sound velocities of hcp Fe-Mg alloys still differ significantly from those of the core as provided by seismic observations, even at 10% Mg content. We showed that at the conditions of the inner core 5-10% Mg stabilizes bcc Fe both dynamically and thermodynamically, and we gave an electronic structure explanation of this phenomenon. We demonstrated that the physical properties of bcc Fe-Mg alloys containing 5-10% Mg reproduce those of the inner core: the calculated density, elastic moduli and sound velocities of bcc Fe-Mg alloys are consistent with seismic data. Therefore the bcc-structured Fe-Mg alloy is amongst the strongest candidate models for the Earth's solid inner core.

6. Acknowledgments

The Kami Research Foundation, the Swedish Research Council, the Swedish Foundation for Strategic Research, the Swedish Energy Agency, the Swedish Foundation for International Cooperation in Research and Higher Education, and the China Scholarship Council are acknowledged for financial support. The calculations were performed on UPPMAX and HPC2N resources.

7. References

Ahuja, B. L., Arora, G., Ahmed, G., Rathor, A., Sharma, V., Kádas, K. & Ahuja, R. (2009). A study of electron momentum density and charge transfer in W-Cu system, *J. Alloys and Comp.* 467: 595–599.

Allegre, C. J., Poirier, J. P., Humler, E. & Hofmann, A. W. (1995). The chemical-composition of the Earth, *Earth Planet. Sci. Lett.* 134(3-4): 515–526.

Andersen, O. K., Arcangeli, C., Tank, R. W., Saha-Dasgupta, T., Krier, G., Jepsen, O. & Dasgupta, I. (1998). *in: Tight-Binding Approach to Computational Materials Science, edited by P. E. A. Turchi and A. Gonis and L. Colombo, MRS Symposia Proceedings No. 491*, Materials Research Society, Pittsburgh. pp. 3–34.

Andersen, O. K., Jepsen, O. & Krier, G. (1994). *in: Lectures on Methods of Electronic Structure Calculations, edited by O. K. Andersen and A. Mookerjee*, World Scientific, Singapore. pp. 63.

Anderson, D. (1989). *Theory of Earth*, Blackwell Scientific Publications, Oxford. pp. 366.

Belonoshko, A. B., Ahuja, R. & Johansson, B. (2003). Stability of the body-centered-cubic phase of iron in the Earth's inner core, *Nature* 424: 1032–1034.

Belonoshko, A. B., Skorodumova, N. V., Davis, S., Osiptsov, A. N., Rosengren, A. & Johansson, B. (2007). Origin of the low rigidity of the Earth's inner core, *Science* 316: 1603–1605.

Belonoshko, A. B., Skorodumova, N. V., Rosengren, A. & Johansson, B. (2008). Elastic anisotropy of Earths inner core, *Science* 319: 797–800.

Birch, F. (1961). Composition of the Earth's mantle, *Geophys. J. Royal Astronomical Soc.* 4: 295–311.

Chen, B., Gao, L., Funakoshi, K. I. & Li, J. (2007). Thermal expansion of iron-rich alloys and implications for the Earth's core, *Proc. Natl. Acad. Sci. USA* 104: 9162–9167.

Cieslak, J., Dubiel, S. M. & Sepiol, B. (2000). Mossbauer-effect study of the phase separation in the Fe-Cr system, *J. Phys.: Condens. Matter.* 12: 6709–6717.

de Boer, F. R., Boom, R., Mattens, W. C. M., Miedema, A. R. & Niessen, A. K. (1988). *Cohesion in Metals: Transition Metal Alloys, Vol. 1, edited by F. R. de Boer and D. G. Pettifor*, North-Holland, Amsterdam.

Delczeg-Czirjak, E. K., Delczeg, L., Ropo, M., Kokko, K., Punkkinen, M. P. J., Johansson, B. & Vitos, L. (2009). Ab initio study of the elastic anomalies in Pd-Ag alloys, *Phys. Rev. B* 79: 085107.

Dorofeev, G. A., Elsukov, E. P. & Ul'yanov, A. L. (2004). Mechanical alloying of immiscible elements in the Fe-Mg system, *Inorg. Mater.* 40: 690–699.

Dubrovinskaia, N., Dubrovinsky, L., Kantor, I., Crichton, W. A., Dmitriev, V., Prakapenka, V., Shen, G., Vitos, L., Ahuja, R., Johansson, B. & Abrikosov, I. A. (2005). Beating the miscibility barrier between iron group elements and magnesium by high-pressure alloying, *Phys. Rev. Lett.* 95: 245502.

Dubrovinskaia, N., Dubrovinsky, L. & McCammon, C. (2004). Iron-magnesium alloying at high pressures and temperatures, *J. Phys. Cond. Mat.* 16: S1143–S1150.

Dubrovinsky, L., Dubrovinskaia, N., Narygina, O., Kantor, I., Kuznetzov, A., Prakapenka, V. B., Vitos, L., Johansson, B., Mikhaylushkin, A. S., Simak, S. I. & Abrikosov, I. A. (2007). Body-centered cubic iron-nickel alloy in Earth's core, *Scince* 316: 1880–1883.

Dubrovinsky, L. S., Saxena, S. K., Tutti, F., Rekhi, S. & LeBehan, T. (2000). In-situ X-ray study of thermal expansion and phase transition of iron at multimegabar pressure, *Phys. Rev. Lett.* 84: 1720–1723.

Dziewonski, A. M. & Anderson, D. L. (1981). Preliminary reference Earth model, *Phys. Earth*

Planet. Inter. 25: 297–356.
Grimvall, G. (1976). Polymorphism of metals .3. theory of temperature-pressure phase-diagram of iron, *Phys. Scr.* 13: 59–64.
Grimvall, G. (1999). *Thermophysical Properties of Materials*, Elsevier, North-Holland, Amsterdam. pp. 70-78.
Gyorffy, B. L. (1972). Coherent-potential approximation for a nonoverlapping-muffin-tin-potential model of random substitutional alloys, *Phys. Rev. B* 5: 2382–2384.
Haitani, T., Tamura, Y., Motegi, T., Kono, N. & Tamehiro, H. (2003). Solubility of iron in pure magnesium and cast structure of Mg-Fe alloy, *Mater. Sci. Forum* 419-422: 697–702.
Hashin, Z. & Shtrikman, S. (1962). A variational approach to the theory of the elastic behaviour of polycrystals, *J. Mech. Phys. Solids* 10: 343–352.
Hemley, R. J. & Mao, H. K. (2001). In-situ studies of iron under pressure: new windows on the Earth's core, *Int. Geol. Rev.* 43: 1–30.
Hightower, A., Fultz, B. & R. C. Bowman, J. (1997). Mechanical alloying of fe and mg, *J. Alloys Compd.* 252: 238–244.
Hill, R. (1952). The elastic behaviour of a crystalline aggregate, *Proc. Phys. Soc. A* 65: 349–354.
Hohenberg, P. & Kohn, W. (1964). Inhomogeneous electron gas, *Phys. Rev.* 136: B864–B871.
Hu, Q., Kádas, K., Hogmark, S., Yang, R., Johansson, B. & Vitos, L. (2007). Predicting hardness of covalent/ionic solid solution from first principles theory, *Appl. Phys. Lett.* 91: 121918.
Hu, Q. M., Kádas, K., Hogmark, S., Yang, R., Johansson, B. & Vitos, L. (2008). Hardness and elastic properties of covalent/ionic solid solutions from first-principles theory, *J. Appl. Phys.* 103: 083505.
Huang, L., Vitos, L., Kwon, S. K., Johansson, B. & Ahuja, R. (2006). Thermoelastic properties of random alloys from first-principles theory, *Phys. Rev. B* 73: 104203.
Hultgren, R., Desai, P. D., Hawkins, D. T., Gleiser, M. & Kelley, K. K. (1973). *Selected Values of the Thermodynamic Properties of Binary Alloys*, American Society for Metals, Metals Park, Ohio. pp. 694-703.
Kádas, K., Lindquist, M., Erikssson, O., Johansson, B. & Vitos, L. (2009). Magnetism-driven anomalous surface alloying between Cu and Cr, *Appl. Phys. Lett.* 94: 172507.
Kádas, K., Vitos, L. & Ahuja, R. (2008a). Elastic properties of iron-rich hcp Fe-Mg alloys up to Earth's core pressures, *Earth Planet. Sci. Lett.* 271: 221–225.
Kádas, K., Vitos, L. & Ahuja, R. (2008b). Theoretical evidence of a superconducting transition in doped silicon and germanium driven by a variation of chemical composition, *Appl. Phys. Lett.* 92: 052505.
Kádas, K., Vitos, L., Johansson, B. & Ahuja, R. (2009). Stability of body-centered cubic iron-magnesium alloys in the Earth's inner core, *Proc. Natl. Acad. Sci. USA* 106: 15560–15562.
Kantor, A. P., Kantor, I. Y., Kurnusov, A. V., Kuznetsov, A. Y., Dubrovinskaia, N. A., Krisch, M., Bossak, A. A., Dmitriev, V. P., Urusov, V. S. & Dubrovinsky, L. S. (2007). Sound wave velocities of fcc Fe-Ni alloy at high pressure and temperature by mean of inelastic X-ray scattering, *Phys. Earth Planet. Inter.* 164: 83–89.
Kohn, W. & Sham, L. J. (1965). Self-consistent equations including exchange and correlation effects, *Phys. Rev.* 140: A1133–A1138.
Kollár, J., Vitos, L. & Skriver, H. L. (2000). *in: Electronic Structure and Physical Properties of Solids: the uses of the LMTO method, Editor H. Dreyssé, Lectures Notes in Physics*,

Springer-Verlag, Berlin. pp. 85.
Korzhavyi, P. A., Ruban, A. V., Abrikosov, I. A. & Skriver, H. L. (1995). Madelung energy for random metallic alloys in the coherent potential approximation, *Phys. Rev. B* 51: 5773–5780.
Korzhavyi, P. A., Ruban, A. V., Odqvist, J., Nilsson, J.-O. & Johansson, B. (2009). Electronic structure and effective chemical and magnetic exchange interactions in bcc Fe-Cr alloys, *Phys. Rev. B* 79: 054202.
Labusch, R. (1972). Statistical theories of solid solution hardening, *Acta Metall.* 20: 917–927.
Laio, A., Bernard, S., Chiarotti, G. L., Scandolo, S. & Tosatti, E. (2000). Physics of iron at Earth's core conditions, *Science* 287: 1027–1030.
Landa, A., Chang, C.-C., Kumta, P. N., Vitos, L. & Abrikosov, I. A. (2002). Phase stability of $Li(Mn_{100-x}Co_x)o_2$ oxides: an ab initio study, *Solid State Ionics* 149: 209–215.
Lin, J. F., Heinz, D. L., Campbell, A. J., Devine, J. M. & Shen, G. (2002). Iron-silicon alloy in Earth's core?, *Science* 295: 313–315.
Magyari-Köpe, B., Grimvall, G. & Vitos, L. (2002). Elastic anomalies in Ag-Zn alloys, *Phys. Rev. B* 66: 064210.
Magyari-Köpe, B., Vitos, L., G. Grimvall, B. J. & Kollár, J. (2002). Low-temperature crystal structure of CaSiO3 perovskite: An ab initio total energy study, *Phys. Rev. B* 65: 193107.
Magyari-Köpe, B., Vitos, L. & Grimvall, G. (2004). Anomalous behavior of lattice parameters and elastic constants in hcp Ag-Zn alloys, *Phys. Rev. B* 70: 052102.
Magyari-Köpe, B., Vitos, L., Johansson, B. & Kollár, J. (2001). Parametrization of perovskite structures: an ab initio study, *Acta Crystallogr., Sect. B: Struct. Sci* 57: 491–496.
Magyari-Köpe, B., Vitos, L., Johansson, B. & Kollár, J. (2002). High-pressure structure of ScAlO3 perovskite, *J. Geophys. Res.-Solid Earth* 107: 2136–2141.
Mao, H. K., Shu, J., Shen, G., Hemley, R. J., Li, B. & Singh, A. K. (1998). Elasticity and rheology of iron above 220 GPa and the nature of the Earth's inner core, *Nature* 396: 741–743.
Mao, H. K., Wu, Y., Chen, L. C. & Shu, J. F. (1990). Static compression of iron to 300 GPa and $Fe_{0.8}Ni_{0.2}$ alloy to 260 GPa: implications for composition of the core, *J. Geophys. Res.* 95: 21737–21742.
Massalski, T. B. (1986). *Binary Alloy Phase Diagrams, edited by T. B. Massalski*, American Society for Metals, Metals Park, Ohio. Vol.1.
Massalski, T. B. (1996). *in: Physical Metallurgy, Structure and Stability of Alloys, Vol.1, edited by R. W. Cahn and P. Haasen*, North-Holland, Amsterdam. pp. 134.
Matsui, M. & Anderson, O. L. (1997). The case for a body-centered cubic phase (α') for iron at inner core conditions, *Phys. Earth Planet. Inter.* 103: 55–62.
McDonough, W. F. (2003). *in: Treatise on geochemistry, Editor R. W. Carlson*, Elsevier, New York. pp. 547-568.
McDonough, W. F. & Sun, S. S. (1995). The composition of the Earth, *Chem. Geol.* 120: 223–253.
Mikhaylushkin, A. S., Simak, S. I., Dubrovinsky, L., Dubrovinskaia, N., Johansson, B. & Abrikosov, I. A. (2007). Pure iron compressed and heated to extreme conditions, *Phys. Rev. Lett.* 99: 165505.
Moruzzi, V. L., Janak, J. F. & Schwarz, K. (1988). Calculated thermal properties of metals, *Phys. Rev. B* 37: 790–799.
Oguchi, T., Terakura, K. & Hamada, N. (1983). Magnetism of iron above the Curie temperature, *J. Phys. F: Met. Phys.* 13: 145–160.
Olsson, P., Abrikosov, I. A., Vitos, L. & Wallenius, J. (2003). Ab initio formation energies of

Fe-Cr alloys, *J. Nucl. Mater.* 321: 84–90.
Olsson, P., Abrikosov, I. A. & Wallenius, J. (2006). Electronic origin of the anomalous stability of fe-rich bcc Fe-Cr alloys, *Phys. Rev. B* 73: 104416.
Pearson, W. B. (1958). *A handbook of lattice spacings and structures of metals and alloys*, Pergamon Press, Belfast. pp. 532.
Perdew, J. P., Burke, K. & Ernzerhof, M. (1996). Generalized gradient approximation made simple, *Phys. Rev. Lett.* 77: 3865–3868.
Pugh, S. F. (1954). XCII. relations between the elastic moduli and the plastic properties of polycrystalline pure metals, *Philos. Mag.* 45: 823–843.
Qiu, S. L. & Marcus, P. M. (2003). Elasticity of hcp nonmagnetic Fe under pressure, *Phys. Rev. B* 68: 054103.
Reuss, A. (1929). Calculating the limit of mishkristallen flowing due to the plastizitatsbeding for monocrystals, *Z. Angew. Math. Phys.* 9: 49.
Robie, R. A., Hemingway, B. S. & Fisher, J. R. (1978). *Thermodynamic properties of minerals and related substances at 298.15 K and 1 bar (105 pascals) pressure and at higher temperatures*, U.S. Geological Survey Bulletin 1452, Washington.
Ross, W., Young, D. A. & Grover, R. (1990). Theory of the iron phase diagram at Earth core conditions, *J. Geophys. Res.* 95: 21713–21716.
Sahlberg, M., Beran, P., Nielsen, T. K., Cerenius, Y., Kádas, K., Punkkinen, M. P. J., Vitos, L., Eriksson, O., Jensen, T. R. & Andersson, Y. (2009). A new material for hydrogen storage; $ScAl_{0.8}Mg_{0.2}$, *J. Solid State Chem.* 182: 3113–3117.
Singh, A. K., Mao, H. K., Shu, J. & Hemley, R. J. (1998). Estimation of single-crystal elastic moduli from polycrystalline X-ray diffraction at high pressure: application to FeO and iron, *Phys. Rev. Lett.* 80: 2157–2160.
Söderlind, P., Moriarty, J. A. & Wills, J. M. (1996). First-principles theory of iron up to earth-core pressures: Structural, vibrational, and elastic properties, *Phys. Rev. B* 53: 14063–14072.
Soven, P. (1967). Coherent-potential model of substitutional disordered alloys, *Phys. Rev.* 156: 809–813.
Speich, G. R., Schwoeble, A. J. & Leslie, W. C. (1972). Elastic constants of binary iron-base alloys, *Metall. Trans.* 3: 2031–2037.
Steinle-Neumann, G., Stixrude, L. & Cohen, R. E. (1999). First-principles elastic constants for the hcp transition metals Fe, Co, and Re at high pressure, *Phys. Rev. B* 60: 791–799.
Steinle-Neumann, G., Stixrude, L., Cohen, R. E. & Gülseren, O. (2001). Elasticity of iron at the temperature of the Earth's inner core, *Nature* 413: 57–60.
Stixrude, L. & Cohen, R. E. (1995). High-pressure elasticity of iron and anisotropy of Earth's inner core, *Science* 267: 1972–1975.
Sutton, A. L. & Hume-Rothery, W. (1955). *Philos. Mag.* 46: 1295–1309.
Taga, A., Vitos, L., Johansson, B. & Grimvall, G. (2005). Ab initio calculation of the elastic properties of $Al_{1-x}Li_x$ ($x \leq 0.2$) random alloys, *Phys. Rev. B* 71: 014201.
Tavaresa, S. S. M., de Noronha, R. F., da Silva, M. R., Neto, J. M. & Pairis, S. (2001). *Mater. Res.* 4: 237.
Vitos, L. (2001). Total-energy method based on the exact muffin-tin orbitals theory, *Phys. Rev. B* 64: 014107.
Vitos, L. (2007). *The EMTO Method and Applications, in: Computational Quantum Mechanics for Materials Engineers*, Springer-Verlag, London.
Vitos, L., Abrikosov, I. A. & Johansson, B. (2001). Anisotropic lattice distortions in random

alloys from first-principles theory, *Phys. Rev. Lett.* 87: 156401.
Vitos, L. & Johansson, B. (2007). Applied parallel computing. state of the art in scientific computing, lecture notes in computer science, springer-verlag berlin heidelberg, B. kagström et al. (eds.), 4699: 510–519.
Vitos, L., Korzhavyi, P. A. & Johansson, B. (2002). Elastic property maps of austenitic stainless steels, *Phys. Rev. Lett.* 88: 155501.
Vitos, L., Korzhavyi, P. A. & Johansson, B. (2003). Stainless steel optimization from quantum mechanical calculations, *Nat. Mater.* 2: 25–28.
Vitos, L., Korzhavyi, P. A. & Johansson, B. (2006). Evidence of large magnetostructural effects in austenitic stainless steels, *Phys. Rev. Lett.* 96: 117210.
Vitos, L., Skriver, H. L., Johansson, B. & Kollár, J. (2000). Application of the exact muffin-tin orbitals theory: the spherical cell approximation, *Comp. Mat. Sci.* 18: 24–38.
Voigt, W. (1889). The relation between the two elastic moduli of isotropic materials, *Ann. Phys. (Leipz.)* 38: 573.
Vočadlo, L. (2007). Ab initio calculations of the elasticity of iron and iron alloys at inner core conditions: Evidence for a partially molten inner core?, *Earth Planet. Sci. Lett.* 254: 227–232.
Vočadlo, L., Alfè, D., Gillan, M. J., Wood, I. G., Brodholt, J. P. & Price, G. D. (2003). Possible thermal and chemical stabilization of body-centered-cubic iron in the Earth's core, *Nature* 424: 536–539.
Vočadlo, L., Brodholt, J., Alfè, D., Gillan, M. J. & Price, G. D. (2000). Ab initio free energy calculations on the polymorphs of iron at core conditions, *Phys. Earth Planet. Inter.* 117: 123–137.
Vočadlo, L., Dobson, D. P. & Wood, I. G. (2006). An ab initio study of nickel substitution into iron, *Earth Planet. Sci. Lett.* 248: 147–152.
Yelsukov, E. P., Dorofeev, G. A. & Ul'yanov, A. L. (2005). Mechanism and kinetics of mechanical alloying in an immiscible Fe-Mg system, *Czech. J. Phys.* 55: 913–920.
Young, D. A. (1991). *Phase Diagrams of the Elements*, University of California Press, Berkeley.
Zander, J., Sandström, R. & Vitos, L. (2007). Modelling mechanical properties for non-hardenable aluminium alloys, *Comp. Mat. Sci.* 41: 86–95.
Zhang, H. L., Johansson, B. & Vitos, L. (2009). Ab initio calculations of elastic properties of bcc Fe-Mg and Fe-Cr random alloys, *Phys. Rev. B* 79: 224201.
Zhang, H. L., Punkkinen, M. P. J., Johansson, B., Hertzman, S. & Vitos, L. (2010). Single-crystal elastic constants of ferromagnetic bcc Fe-based random alloys from first-principles theory, *Phys. Rev. B* 81: 184105.

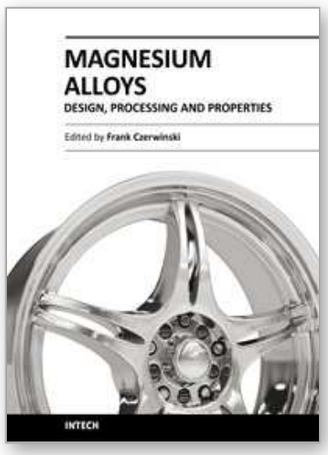

Magnesium Alloys - Design, Processing and Properties

Edited by Frank Czerwinski

ISBN 978-953-307-520-4
Hard cover, 526 pages
Publisher InTech
Published online 14, January, 2011
Published in print edition January, 2011

Scientists and engineers for decades searched to utilize magnesium, known of its low density, for light-weighting in many industrial sectors. This book provides a broad review of recent global developments in theory and practice of modern magnesium alloys. It covers fundamental aspects of alloy strengthening, recrystallization, details of microstructure and a unique role of grain refinement. The theory is linked with elements of alloy design and specific properties, including fatigue and creep resistance. Also technologies of alloy formation and processing, such as sheet rolling, semi-solid forming, welding and joining are considered. An opportunity of creation the metal matrix composite based on magnesium matrix is described along with carbon nanotubes as an effective reinforcement. A mixture of science and technology makes this book very useful for professionals from academia and industry.

InTech Europe
University Campus STeP Ri
Slavka Krautzeka 83/A
51000 Rijeka, Croatia
Phone: +385 (51) 770 447
Fax: +385 (51) 686 166
www.intechopen.com

InTech China
Unit 405, Office Block, Hotel Equatorial Shanghai
No.65, Yan An Road (West), Shanghai, 200040, China
中国上海市延安西路65号上海国际贵都大饭店办公楼405单元
Phone: +86-21-62489820
Fax: +86-21-62489821

IntechOpen